Title
The evaluation of a multiphasic 3D-bioplotted scaffold seeded with adipose derived stem cells to repair osteochondral defects in a porcine model

Journal
Journal of Biomedical Materials Research Part B Applied Biomaterials, 109(12)

ISSN
1552-4973

Authors
Nordberg, Rachel C
Huebner, Pedro
Schuchard, Karl G
et al.

Publication Date
2021-12-01

DOI
10.1002/jbm.b.34886

Peer reviewed

HHS Public Access

Author manuscript

J Biomed Mater Res B Appl Biomater. Author manuscript; available in PMC 2021 December 01.

Published in final edited form as:

J Biomed Mater Res B Appl Biomater. 2021 December ; 109(12): 2246–2258. doi:10.1002/jbm.b.34886.

The evaluation of a multiphasic 3D-bioplotted scaffold seeded with adipose derived stem cells to repair osteochondral defects in a porcine model

Rachel C. Nordberg[#1,2], **Pedro Huebner**[#3,4,5], **Karl G. Schuchard**[3,4], **Liliana F. Mellor**[2], **Rohan A. Shirwaiker**[2,3,4], **Elizabeth G. Loboa**[1,6], **Jeffery T. Spang**[7]

[1]College of Engineering, University of Missouri, Columbia, Missouri

[2]Joint Department of Biomedical Engineering, University of North Carolina at Chapel Hill and North Carolina State University, Raleigh, North Carolina

[3]Department of Industrial and Systems Engineering, North Carolina State University, Raleigh, North Carolina

[4]Comparative Medicine Institute, North Carolina State University, Raleigh, North Carolina

[5]School of Industrial and Systems Engineering, University of Oklahoma, Norman, Oklahoma

[6]Office of the Provost, Southern Methodist University, Dallas, Texas

[7]Department of Orthopaedics, University of North Carolina School of Medicine, Chapel Hill, North Carolina

[#] These authors contributed equally to this work.

Abstract

There is a need for the development of effective treatments for focal articular cartilage injuries. We previously developed a multiphasic 3D-bioplotted osteochondral scaffold design that can drive site-specific tissue formation when seeded with adipose-derived stem cells (ASC). The objective of this study was to evaluate this scaffold in a large animal model. Osteochondral defects were generated in the trochlear groove of Yucatan minipigs and repaired with scaffolds that either contained or lacked an electrospun tidemark and were either unseeded or seeded with ASC. Implants were monitored via computed tomography (CT) over the course of 4 months of in vivo implantation and compared to both open lesions and autologous explants. ICRS II evaluation indicated that defects with ASC-seeded scaffolds had healing that most closely resembled the aulogous explant. Scaffold-facilitated subchondral bone repair mimicked the structure of native bone tissue, but cartilage matrix staining was not apparent within the scaffold. The open lesions had the highest volumetric infill detected using CT analysis ($p < 0.05$), but the repair tissue was largely disorganized. The acellular scaffold without a tidemark had significantly more volumetric filling than either the acellular or ASC seeded groups containing a tidemark ($p < 0.05$), suggesting

Correspondence: Elizabeth G. Loboa, Office of the Provost, Southern Methodist University, Dallas, TX 75275, USA. egloboa@smu.edu, Jeffery T. Spang, Department of Orthopaedics, University of North Carolina School of Medicine, Chapel Hill, NC 27599, USA. jspang@med.unc.edu.

CONFLICT OF INTEREST

The authors declare no potential conflict of interest.

that the tidemark limited cell infiltration into the cartilage portion of the scaffold. Overall, scaffold groups repaired the defect more successfully than an open lesion but achieved limited repair in the cartilage region. With further optimization, this approach holds potential to treat focal cartilage lesions in a highly personalized manner using a human patient's own ASC cells.

Keywords

in vivo; osteochondral; stem cells; tissue engineering; 3D-printing

1 | INTRODUCTION

Osteoarthritis (OA) is characterized by the degeneration of articular cartilage and the underlying subchondral bone. OA is a highly debilitating disease with a global age-standardized prevalence of 3.8% in the knee and 0.85% in the hip.[1] OA is a degenerative disease that often affects the elderly population,[1] but also can develop due to focal cartilage damage from traumatic events such as sports injuries.[2] Current therapies for treating focal osteochondral defects include microfracture, autologous osteochondral grafting, and matrix-assisted autologous chondrocyte implantation (MACI).[3] However, these procedures have several disadvantages. Microfracture results in fibrocartilage formation rather than functional articular cartilage, autologous grafting is associated with high donor site morbidity and limited graft availability, and MACI requires two separate surgeries to be implemented and its efficacy is often inconsistent.[4,5] If the focal defect progresses to OA, a total joint replacement may be necessary.[4,5] While these treatments offer some clinical relief, recent advances in tissue engineering may yield additional treatment options for patients suffering from focal cartilage lesions.

Several challenges exist toward developing tissue-engineered cartilage repair therapies. First, unlike bone, cartilage has limited self-repair capacity, and many factors impede the integration of implanted cartilage.[6] Thus, it is challenging to generate cartilage-only tissue-engineered constructs that can integrate with the surrounding tissue. Second, identifying a reliable cell source for cell-based tissue engineering approaches is a challenge because the isolation of chondrocytes from healthy tissue causes donor site morbidity, and chondrocytes dedifferentiate during in vitro expansion.[7] To circumvent cell-sourcing issues, stem cells such as relatively accessible adipose-derived stem cells (ASC) have been used,[8] although these require in vitro differentiation. Finally, there is a complex interplay between articular cartilage and the underlying subchondral bone. Cartilage damage and degeneration are often accompanied by degeneration of the subchondral bone, and vitality of the overlying cartilage relies heavily on the health of the subchondral bone.[9] Tissue engineering the osteochondral unit as a whole may effectively repair damaged cartilage tissue.

Several osteochondral scaffolds have been generated using biphasic designs consisting of an osteoinductive base and a collagen surface.[10–14] Biphasic scaffolds circumvent some of the challenges associated with cartilage integration as they can be press fit into an osteochondral defect and integrate with the subchondral bone. To induce cartilage and bone formation simultaneously, other scaffolds have been designed by introducing biomimetic

factors in a site-specific manner.[15,16] For example, one group has investigated the use of bio-mineralized collagen and hyaluronic acid-charged collagen to engineer the subchondral bone and cartilage regions, respectively.[16] A graded transition from bone to cartilage to reduce shear stresses at the biomaterial interfaces has also been investigated for osteochondral scaffold design.[16–22] An agarose hydrogel containing polylactide-co-glycolide and 45S5 bioactive glass microspheres has been generated with regions that replicate the cartilage, calcified cartilage, and bone regions of osteochondral tissue.[17] Others have generated a graded nano-composite scaffold via nucleating collagen fibrils with hydroxyapatite nanoparticles.[20] Recently, we generated a 3D-bioplotted scaffold that incorporated both β-tricalcium phosphate (TCP) and decellularized cartilage extracellular matrix (dECM) to induce site-specific differentiation of human adipose stem cells (hASC) as a single cell source.[23] Specifically, 20% TCP was incorporated into a polycaprolactone (PCL) base to induce osteogenic differentiation of ASC. The chondrogenic side consisted of PCL pores infused with dECM. Both layers were 3D printed using a design that we previously optimized.[24] Additionally, we incorporated an electrospun layer between the bone and cartilage layers to mimic the natural tidemark found in osteochondral tissue.[23] This tidemark layer was added to maintain separation between the layers and prevent blood vessel and ossification of the cartilage tissue, which has been documented as a challenge for in vivo success.[25] While in vitro assessment of this scaffold design was promising, the capacity of the construct to repair osteochondral tissue required in vivo evaluation in a large animal model.

Therefore, the objective of this study was to evaluate our previously developed osteochondral scaffold[23] for integration and tissue repair in the translationally relevant Yucatan minipig model. Large animal studies are crucial for evaluating the translational potential of osteochondral implants because they can replicate the design characteristics of a human implant in terms of cartilage thickness and surgical techniques used. Moreover, large animal models provide a more biologically accurate environment to assess cartilage repair because small animal models have an intrinsic capacity for cartilage repair, which predisposes such models to favorable outcomes that would not translate to the human. The Yucatan minipig is a promising large animal model for cartilage repair because the minipig has similar load-bearing and anatomical characteristics to the human knee.[26,27] Allogeneic Yucatan minipig ASC (pASC) were used as the cell source for this study, to mimic our intended human cell source of hASC. Five experimental groups were created and evaluated: (1) open lesion (negative control); (2) acellular construct with no electrospun tidemark; (3) acellular construct with an electrospun tidemark; (4) pASC-seeded construct with an electrospun tidemark; and, (5) autologous explant (positive control). We hypothesized that the inclusion of an electrospun tidemark and seeding with pASC would most successfully repair osteochondral lesions relative to all other experimental groups and most closely mimic the positive control autologous explant.

2 | MATERIALS AND METHODS

2.1 | Study design

Two defects were created in the trochlear groove of both hind limbs of seven minipigs, creating a total of 28 osteochondral defects. Surgeries were carried out in two phases: two pigs were used in Phase 1, and five pigs were used in Phase 2 (Figure 1(a)). During this two-phase study, defect sites were assigned to five groups: open lesion ($n = 7$), acellular scaffold no tidemark ($n = 5$), acellular scaffold tidemark ($n = 6$), pASC seeded scaffold ($n = 5$), autologous explant ($n = 5$). Phase 1 consisted of only acellular scaffolds, while Phase 2 consisted of both seeded and acellular scaffolds. To obtain cells from Phase 2, subcutaneous adipose tissue was collected from the belly after the animals of Phase 1 were sacrificed. Experimental groups were not repeated within the same animal, and each animal received an open lesion negative control. Experimental groups were assigned at random to each implant location. The sample size of $n = 5$ or greater per group was determined using power analysis, $\alpha = 0.05$, power = 0.8, and a standard deviation of 25, and a desired effect size to detect of 50. Values were determined from previously reported ICRS-II cartilage repair data in the same animal model.[28]

2.2 | Scaffold fabrication

Pre-fabrication, stereolithography (STL) files were prepared using SolidWorks (Dassault Systèmes SOLIDWORKS Corp., Waltham, MA). The osteogenic phase (portion of scaffold representing subchondral bone) was designed as a cylinder (Ø 7.9 × 4 mm) with a 1 mm, 30° chamfer incorporated at the bottom edge to facilitate positioning during the surgical implantation procedure. The chondrogenic phase was designed as a disc (Ø 7.9 × 2 mm). Full-thickness scaffolds were fabricated using a 3D-Bioplotter (EnvisionTEC GmbH, Gladbeck, Germany) set up with two distinct materials: 100% PCL (M_W = 45 kDa, Poly-sciences, Inc., Warrington, PA) for the chondrogenic phase, and a homogenous blend of 80% PCL and 20% TCP (Riedel-de Haën, Seelze, Germany), by weight, for the osteogenic phase. A summary of microarchitectural and process parameters is presented in Table 1.

To represent the tidemark phase, electrospun PCL matrices were generated using methods we have previously developed and described.[15,23,29–32] Briefly, PCL dissolved in chloroform and dimethylformamide at a volumetric ratio of 3:1 for 4 hr at 80°C was electrospun at a feed rate of 0.7 μl/h, voltage of 15 kV, and spinning distance of 13–15 cm. The electrospun matrices were collected onto a static collector covered with aluminum, then cut into Ø 8-mm disks using a standard gasket hole punch tool.

The full-thickness scaffold was fabricated upside down with respect to its implantation orientation. The chondrogenic phase (PCL) was bioplotted first. Then, for scaffolds featuring a tidemark-mimicking layer, an electrospun PCL disk was overlaid on top of the chondrogenic phase. Finally, the osteogenic phase (PCL-TCP) was bioplotted on top. Post-fabrication, scaffolds were inspected under a digital microscope to verify their microstructural integrity and to measure select properties of the strand microarchitecture, namely the mean strand width and interstrand spacing. In addition, three measurements of

the diameter and height of each scaffold were randomly obtained using a digital precision caliper to determine their bulk dimensional characteristics.

2.3 | Cell culture and scaffold seeding

In vitro scaffold preparation was adapted from our previously reported methods[23] to rely on purely porcine components (extracellular matrix and cell source).

Extracellular matrix derived from porcine hock joints (Nahunta Pork Center, Pikeville, NC) was used in a hydrogel form as a constituent of the 3D-bioplotted scaffolds for the chondrogenic phase, as described previously.[23] Briefly, cartilage was harvested from fresh porcine hock joints. Native cells were lysed via hypotonic shock by suspending tissue in a solution of deionized water and 0.5% penicillin/streptomycin and mixing for 24 hr to generate dECM. The cartilage dECM was then frozen in 1X PBS and lyophilized for 24 hr. The lyophilized cartilage was pulverized in a mill using a number 40 size mesh to obtain the cartilage dECM powder. The dECM gels were prepared at an initial concentration of 25 mg/ml. The ECM was digested for 48 hr in a 2 mg/ml solution of pepsin in 0.1 M HCL. 4 ml of this solution was added to 100 mg of cartilage dECM powder. 400 μl of 1 M NaOH was added to the solution to bring the pH to 7.4. Finally, 489 μl of 10X PBS was added to the solution to make the concentrations of NaOH, HCl, and PBS equal to each other. The final concentration of the gel was calculated to be 20.5 mg/ml.

ASC were isolated and expanded as previously described[33,34] in complete growth medium (CGM) comprised of alpha-modified minimal essential medium (α-MEM with L-glutamine) (Invitrogen, Carlsbad CA), 10% fetal bovine serum (FBS) (Premium Select, Atlanta Biologicals, Lawrenceville GA), 200 mM L-glutamine, and 100 I.U. penicillin/100 μg/ml streptomycin (Mediatech, Herndon VA). Porcine ASC were cultured (37°C, 5% CO2) until reaching 80% confluency changing the media every 3 days, and then passaged using trypsin–EDTA (Invitrogen). All experiments were run using pASC at passage 2.

A two-day pASC seeding protocol was used to seed the full thickness scaffolds, as depicted in Figure 1(b). On the first day, the scaffolds were sterilized with successive 70% ethanol and PBS washes. The chondrogenic phase was prepared by submerging the 3D-bioplotted PCL in neutralized dECM solution and incubating at 37°C for 1 hr. After the hydrogel had solidified, the scaffold was flipped chondrogenic PCL phase up, seeded with 7.5×10^4 pASC, and incubated overnight (37°C, 5% CO_2). On the second day, the scaffolds were flipped osteogenic PCL-TCP phase up and seeded with an additional 15×10^4 pASC. Each osteochondral scaffold was then incubated in 3 ml CGM for 28 days. Media was changed, and scaffolds were flipped every 2 days. An image of the finished scaffold is shown in Figure 1(c).

2.4 | Calcium release characterization

Although we have previously reported in vitro characterization of our scaffolds,[23] the dimensions of the scaffold design were modified to accommodate for in vivo implantation, necessitating the characterization of calcium release from our scaffolds. Calcium release assays were performed to characterize release profiles from the PCL-TCP portion of the scaffold. PCL-TCP scaffolds were placed into separate microcentrifuge tubes ($n = 3$ per

time point) and treated for 30 min with 70% ethanol to mimic the sterilization process and increased the hydrophilicity of the scaffolds. The scaffolds were then fully submerged in 1 ml of phosphate buffered saline (PBS) and maintained in an incubator (37°C, 5% CO_2) for the duration of the experiment. PBS was collected at time points of 1, 2, 4, 7, 14, and 28 days and stored at −25°C until assayed. A Calcium LiquiColor® Assay (StanBio, Boerne, TX) was used to quantify the calcium content of each sample.

2.5 | Animal care

All animal procedures were approved by the Institutional Animal Care and Use Committee (IACUC) at North Carolina State University (IACUC No. 16–126). Seven female 7-month-old Yucatan miniature pigs weighing 30–40 kg were obtained from Sinclair Research Center (Auxvasse, MO). The minipig model has been utilized by many research groups in the evaluation of osteochondral defect models.[13,35] Pigs were housed in the NCSU College of Veterinary Medicine Laboratory Animal Resources pig housing on concrete floors with pine shavings bedding on 12 h-12 h light–dark cycle. They were fed a lab diet pig ration to satisfy kcal requirements for breed/age. The pigs were singly housed with access to conspecifics through pen bars. The animals had access to water ad lib through a lixit watering system and were fed twice a day a.m. and p.m.

2.6 | Surgical procedure: implant

The animals were sedated, anesthetized, and cared for post-operatively according to IACUC guidelines at our institution. After standard surgical preparation and draping, a single 7-cm vertical incision was made just inferior to the patella. The underlying tissues were split longitudinally, including the patellar tendon. With differing angles of knee flexion, the trochlear groove was accessed. A commercially available FDA-approved Osteochondral Transfer System (COR Depuy Synthes, Warsaw, IN) was used to create two recipient defects 8 mm in circumference and 6 mm in depth with a stepped reamer and guide. In accordance with preplanned distribution, either scaffolds or autologous explants were inserted using a press-fit technique into the osteochondral defect. The implants were inserted flush to the surrounding articular cartilage. Some defects were left open without a scaffold or autologous explant. The knee was taken through a range of motion to ensure the implants were stable. The paratenon overlying the patellar tendon was closed with an absorb-able suture. The skin was closed with staples, and a sterile dry dressing was placed. In vivo implantation technique is depicted in Figure 2.

2.7 | Surgical procedure: explant

Animals were euthanized, then standard surgical preparation and draping were performed to minimize the risk of cellular contamination. The anterior knee skin incision was opened, allowing the release of the patellar tendon from its insertion. The knee capsule was released on the medial and lateral sides, allowing increased patella mobility and good access to the trochlear groove. For each osteochondral defect, an oscillating saw was used to make perpendicular cuts at least 3 mm from the edge of the defect. An osteotome was used to remove medial and lateral bone allowing transection of the bone 15 mm deep to the articular surface. In this fashion, rectangular osteochondral blocks containing the recipient osteochondral defects were harvested.

2.8 | Gross observation and defects assessment

Upon sacrifice, the joints were opened and high-resolution digital photos of the exposed surface of the osteochondral defect sites were taken for blind grading by four unbiased and independent evaluators with expertise in cartilage biology. The Cartilage Repair Assessment Scoring System (Protocol B) proposed by the International Cartilage Repair Society (ICRS)[36,37] was used to grade the degree of defect repair, integration to the border zone, and the macroscopic appearance of implants, using a methodology similar to that employed by others.[38–40]

2.9 | CT scanning and bone ingrowth assessment

CT scans were taken at days 15, 45, 75, 105, and 120 (harvest). The scan envelope was limited to capture both knee joints and the immediately adjacent length of the femur and tibia/fibula of each animal's hind limbs, which ensured complete imaging of the osteochondral defect sites, implants, and surrounding tissues. A Sensation 16 slice CT scanner (Siemens Medical Solutions, Malvern, PA) was set up with the following scanning parameters: 120 kV, 110 mA, B60s filter, slice thickness 0.75 mm, and a resolution of 512 × 512 pixels per slice resulting in a field of view of approximately 462 cm^2. DICOM files were imported into Mimics Research 19 (Materialise NV, Leuven, Belgium) for biomodelling. Bone tissue was masked using the program's standard thresholding limits for CT scans and bone tissue (HU range: 226–1,686). Any instance of excessive noise within or around the knee joint was removed using manual mask correction tools. 3D meshes were created for the regions within each joint encompassing the defect sites using optimal quality option, then exported as STL files. Using Magics 19 (Materialise NV), STL files were opened individually, and volumetric quantification of the osteochondral defects was performed. In brief, each defect was cut by two parallel planes, wherein the first coincided with the surface of the joint interfacing with the edge of the defect and the second resided deeper into the joint, exactly 8 mm apart from the first one and parallel to it, hence giving the isolated 3D model of the defect a cylinder-like geometry. Finally, the volume of each osteochondral defect was estimated in mm^3, bounded by the two planes mentioned above and the lateral limits of each defect. Results are reported for analysis as the percent defect fill at days 45, 75, 105, and 120 relative to day 15, defined by Equation 1, where v_{15} is the volume of a defect at day 15, and v_{TP} is the volume of that same defect at the later time points. This quantification protocol was inspired by relevant literature on the subjects of bone and cartilage tissue engineering.[28,41,42] Two independent evaluators followed the steps above as a means of pooling for any variability introduced by human error during the process, wherein the results were averaged for analysis.

$$\%DefectFill = \left(\frac{v_{15} - v_{TP}}{v_{15}}\right) * 100 \quad (1)$$

2.10 | Histology and IHC

Upon collection, samples were fixed for 7 days in formalin before undergoing decalcification and sectioning by the NC State Histology core. Safranin-O staining was used to determine the proteoglycan content of the seeded scaffolds. Scaffolds were fixed

in 10% formalin and first stained with Weigert's Iron Hematoxylin stain (Sigma-Aldrich, St. Louis, MO) for 10 min, then rinsed under running tap water. They were then stained with fast green (Sigma-Aldrich) for 5 min and washed in 1% acetic acid, followed by an 8-min Safranin-O (Sigma-Aldrich) stain. Alcian Blue (Sigma-Aldrich) staining was used to determine sulfated glycosaminoglycan (sGAG) content of the seeded scaffolds. After fixation as described above, scaffolds were stained in an Alcian blue solution for 30 min, washed under running tap water for 2 min, and rinsed with deionized water. Scaffolds were then stained with 0.1% Nuclear Fast Red (Sigma-Aldrich) for 5 min, tap water for 1 min. Additional paraffin-embedded slides were used for immunohistochemistry. The protocol used was adapted from previously described methods.[43] In brief, slides were deparaffinized and washed for 20 min in 10 mM citrate antigen retrieval buffer heated to 90°C. The slides were then washed for 10 min in 1x Tris-buffer saline/0.5% Tween 20 solution, 30 min in a 37 units/ml hyaluronidase solution, 30 min in a 3% hydrogen peroxide solution, and blocked with a normal donkey serum solution for 1 hr. Samples were incubated at room temperature for 2 hr in a 1:200 dilution primary antibody solution (rabbit polyclonal Collagen II antibody, Abcam, Cambridge, United Kingdom). The samples were washed with PBS, and incubated in secondary solution for 1 hr (goat anti-rabbit IgG H&L HRP polymer, Abcam). The slides were stained with a DAB Substrate Kit (Abcam) for 10 min. Histological staining was evaluated using a modified ICRS II scoring system as described previously[44] by five unbiased and independent evaluators with expertise in cartilage biology. Only ICRS II parameters that were clearly represented in the histological staining were scored.

2.11 | Statistics

Data were analyzed in PRISM (GraphPad, San Diego) using one- or two-way analysis of Variance (ANOVA) with differences between group means analyzed using Tukey's adjustment for multiple comparisons. All values are reported as mean ± standard deviation. p-values less than 0.05 were considered statistically significant.

3 | RESULTS

3.1 | Scaffold characterization

Strand width, interstrand spacing, scaffold diameter, and scaffold height for each fabricated design are summarized in Table 2. Strand width and separation were within 4% and 10% of nominal values (350 and 650 μm, respectively). No statistically significant differences ($p < 0.05$) were found between the microarchitectural characteristics of the two scaffold designs (strand width and interstrand spacing). Calcium was released from the scaffolds during 28 days in vitro culture. As shown in Figure 1(d), the release rate was steady for the first 2 weeks and then leveled off.

3.2 | Gross repair grading

Representative images of gross morphology and corresponding H&E staining are depicted in Figure 3(a). A summary of the ICRS Cartilage Repair Assessment Scoring System ratings for all experimental groups is presented in Figure 3(b). The autologous explant was rated significantly higher than every group except for the pASC seeded scaffolds ($p < 0.05$).

3.3 | Histological evaluation

Magnified H&E images of surface characteristics, treatment integrations with the surrounding bone, and defect fill are presented in Figure 4. Articular cartilage did not appear to be generated in the treatment groups. However, bone architecture within the defect of the scaffold-treated groups was more similar to the autologous explant than the open lesion, which was filled with unorganized fibrous tissue featuring some degree of mineralization as evidenced by the CT scans. The observed bone structure in the scaffold treated groups was likely provided by the PCL scaffold itself rather than extensive new tissue formation. Higher cell density was observed on the seeded scaffolds, but nuclei staining was observed on the unseeded scaffolds as well, indicating native cell infiltration. All scaffolds were able to integrate with native bone, but the bone from the autologous explant was indistinguishable from the native bone and could only be identified via a discontinuity at the native/explant cartilage interface. Histological images of cartilage matrix components are presented in Figure 5(a). Empty defects formed large recesses filled with disorganized repair tissue. While the positive control (i.e., autologous explant) cartilage aligned with the native tissue, the cartilage zones of the experimental scaffolds did not remain aligned with the native tissue over the course of the 4 months of implantation. Moreover, cartilage matrix staining was not apparent within the scaffold component of the defect. Subchondral bone porosity was observed when a scaffold was used to fill the defect, but not in the open lesion groups. In some samples that included a electrospun layer, (e.g., Figure 5(a), Acellular tidemark, Collagen II IHC) the electrospun layer was evident in the histology. Blind reviewers graded the histological outcomes (Figure 5(b)–(g)) on the ICRS II grading system and, although there was no statistical significance between groups, the positive control scored the highest in all categories (overall assessment, surface/superficial assessment, mid/deep zone assessment, subchondral bone, cartilage matrix staining, and calcification front/tidemark), and pASC-seeded scaffold group most closely mimicked the positive control.

3.4 | Bone ingrowth assessment from CT scans

Figure 6(a) presents examples of 3D biomodels created from CT scan data and used for the volumetric quantification of bone defects, and the mean defect volume ± standard deviation (mm^3) for all experimental groups and time points. Data was analyzed as the percent defect fill at days 45, 75, 105, and 120 relative to day 15. A summary of the results is presented in Figure 6(b). The presence of a positive slope within each experimental group and across time points, as well as predominantly positive values, indicate that bone formation was observed in all cases, despite an initial loss of tissue for scaffold groups featuring a tidemark (“acellular tidemark” and “pASC seeded” groups). Statistically, the effects of both experimental group and time point were found to be significant ($p < 0.001$), but their interaction was not ($p = 0.254$). Table 3 summarizes the post-hoc results of the two-way ANOVA wherein statistically significant differences between experimental groups and time points exist when $p < 0.05$.

In brief, open lesions exhibited the highest volumetric changes across all time points and reached, at day 120, a defect fill of 76.7 ± 27.1% of the defect’s initial volume. Scaffolds from the “acellular no tidemark” group expressed comparably higher defect fill percentages against other scaffold groups, however significantly ($p = 0.001$) lower than their counterparts

in the open lesion group, ultimately reaching 39.9 ± 27.1% at day 120. For the experimental groups featuring scaffolds with a tidemark layer ("acellular tidemark" and "pASC seeded" groups), the percent defect fill was significantly lower than the 'acellular no tidemark' group ($p = 0.016$ and $p < 0.000$, respectively). In fact, the 'acellular tidemark' and 'pASC seeded' groups were the only to express an initial loss of mineralized tissue at day 45 (−5.4 ± 17.7% and − 23.1 ± 26.2%, respectively), but this phe-nomenon was eventually reverted and the average percent defect fill became positive at day 120 (22.3 ± 32.4% and 3.9 ± 30.4%, respectively). Lastly, the "autologous explant" group, which consisted of zero or near-zero defect volume at day 15 for most samples, exhibited the least change over time, with no significant variation between time points.

4 | DISCUSSION

The objective of this study was to evaluate a multiphasic osteochondral scaffold in a minipig model. This study took advantage of recent advances in rapid manufacturing to generate a bioplotted scaffold comprising a TCP phase to induce osteogenic differentiation and a dECM phase to induce chondrogenic differentiation. An electrospun layer was incorporated as a tidemark to separate the bone and cartilage phases of the scaffold and avoid cell infiltration and blood vessel invasion into the cartilage portion of the scaffold. Tissue regeneration was enhanced by the implantation of a scaffold, and tidemark incorporation modulated bone fill. While the bone architecture was more successfully repaired than cartilage architecture, scaffolds manufactured with a tidemark and loaded with pASC received ICRS I and ICRS II scores for cartilage repair that most closely mimicked the positive control.

As expected, defects that were filled via our positive control (i.e., autologous explants) yielded superior healing. Although we were not able to replicate this with scaffold implantation, clinically, an autologous osteochondral transfer generates a secondary defect within the patient, which has operative complications and associated morbidities.[45] A scaffold-based approach would alleviate these issues. Promisingly, the scaffold-filled defects were able to generate tissue with a structure resembling that of subchondral bone, which was improved over open lesion defects, which filled with dense fibrotic tissue. While the scaffold-filled defects were improved over open lesions, a challenge of the current study was that hyaline cartilage was not generated via the implanted scaffold itself. However, in some of the cases, native cartilage filled over the top of the scaffold (see Figure 5) suggesting that, by inhibiting fibrotic repair tissue, the scaffolds were able to facilitate cartilage regeneration.

There are two predominant mechanisms by which ASC may aid in osteochondral defect repair. First, the ASC is able to differentiate and form bone and cartilage cells. We and others have demonstrated that ASC have multilineage differentiation potential and can differentiate toward bone and cartilage lineages.[23,46–48] In this study, we facilitated this mechanism by incorporating biomimetic factors tri-calcium phosphate and decellularized cartilage extracellular matrix to drive osteogenic and chondrogenic differentiation, respectively. We demonstrated previously that tri-calcium phosphate promoted osteogenic differentiation,[15,23,32,49] and cartilage extracellular matrix promoted chondrogenic differentiation.[23] The second mode of action of mesenchymal stem cells is

through the release of immunomodulatory and various trophic factors.[50] ASC have been shown to inhibit peripheral blood mononuclear cell immune responses in a dose-dependent fashion, inhibit lymphocyte response to mitogens, and to help control graft-versus-host disease.[51] In the current study, the scaffolds that contained ASC received higher repair scores than the non-seeded scaffolds when implanted in vivo. This suggests that either ASC differentiated down the osteogenic and chondrogenic lineages to facilitate repair or that the ASC released bioactive factors that modulated the host immune response leading to overall better healing.

A novel aspect of this study was the inclusion of an electrospun layer to mimic a tidemark. Tidemarks are naturally present at the cartilage-bone junction of healthy articular cartilage.[52] In OA, it has been demonstrated that blood vessels penetrate across the compromised tidemark from the bone to the cartilage.[53] However, within the context of osteochondral tissue engineering, tidemarks are often overlooked and producing a tissue-engineered tidemark that mimics native tissue architecture has yet to be achieved. For example, in newly regenerated tissue of a nanofibrous PCL tissue for osteochondral repair, a tidemark is not present.[35] Additionally, minimal success was observed when evaluating de novo tidemark formation within biphasic osteochondral scaffolds in vivo.[13] Since it is difficult to induce tidemark formation in tissue-engineered constructs, we included a tidemark-like phase within the present design through the addition of an electrospun layer. We have previously demonstrated in vitro that the inclusion of an electrospun tidemark inhibits cell migration between phases.[23] In the current study, the inclusion of a tidemark significantly reduced tissue infill from the levels of the open lesion and acellular scaffolds without a tidemark. These data suggest that the tidemark inhibited native cell migration across the osteochondral junction. While further optimization is needed to ensure that the tissue-engineered tidemark aligns with the native tidemark, once refined, this could present a novel method of preventing blood vessel invasion into the cartilaginous portion of osteochondral scaffolds.

While the overall healing was promoted by the scaffolds and cells, the volume of bone filling was diminished. The highest volumetric filling was found in the open lesion, likely due to the fact that no bone component was added to fill the defect allowing more space for repair to occur. However, the organization of the filled tissue was not taken into account in this measurement and the repair tissue observed in the open lesions was fibrotic and did not have porosity typical of subchondral bone. Interestingly, the acellular scaffolds without a tidemark had significantly more volumetric bone filling than either the acellular or pASC-seeded scaffolds that contained a tidemark. This could suggest that the electrospun tidemark layer prevents bone from filling into the cartilaginous portion of the scaffold. This is further supported by histological staining showing a more homogeneous appearance of the scaffolds lacking a tidemark. However, cartilage repair was not as successful as expected, partially because the cartilage portion of the scaffold sank below the cartilage of the native tissue. Nevertheless, this strategy of adding a physical tidemark layer to maintain separation between the cartilage and bone should be further investigated. The volumetric filling was lowest in the pASC seeded group. This could either be because the seeded scaffolds had more tissue at implantation to block bone filling or because the pASC inhibited the invasion of repair tissue through immunomodulatory properties.

There were several limitations of the animal model used for this study. Yucatan minipigs are a popular large animal model for evaluating osteochondral injuries due to size, similarity to the human knee, and easier access to the knee articular cartilage. We elected to use seven-month-old pigs, which allowed appropriate surgical implantation as older pig knees have dense subchondral bone and thinner articular cartilage. Although previous authors placed osteochondral lesions on each side of the trochlear groove,[12] we elected to place one superior and one inferior defect per knee due to the small size of the immature minipig joint. Defects 8 mm in diameter were chosen to mimic surgical techniques and instrumentation currently in use in human patients allowing adaptation to the laboratory environment. Due to the contour of the trochlea and the cartilage thickness of the minipigs, we had difficulty aligning the edges of our cartilage induction layer of the scaffold with native tissue. The epiphyseal plate of the minipigs remained open at the time of implantation, which may have affected healing. Spontaneous cartilage repair in immature pigs has been previously reported.[54] For future studies, the depth of the cartilage induction layer could be adjusted to better mimic the immature minipig knee, or a skeletally mature porcine model could be considered. Furthermore, as a means of better characterizing the effect of time on cartilage formation, we highlight the potential of a modified CT scan acquisition protocol that makes use of contrast materials for cartilage tissue visualization, so as to provide data and analysis more in line with the study presented by Fisher et al.[28]

In conclusion, this is the first study to examine in vivo outcomes of using an osteochondral PCL scaffold that uses TCP and dECM to induce site-specific differentiation of ASC. Lesions filled with scaffolds yielded improved architecture and tissue infill when compared to open lesions. Implants loaded with pASC had the best ICRS II grading among the experimental groups. The incorporation of an electrospun tidemark promoted the maintenance of site-specific boundaries within the construct during in vivo implantation. With further refinement, this approach holds great potential to treat OA patients in a highly personalized manner using a patient's own hASC donor cells.

ACKNOWLEDGEMENTS

This work was supported in part by the OREF Research Grant in Stem Cells and Regenerative Medicine Grant with the National Stem Cell Foundation # 15-059 (JS, EGL, RAS), NIH/NIBIB 1R03EB008790 (EGL), NIH/CTSA 550KR71418 (EGL), NIH/CTSA 550KR61325 (EGL), NSF/CBET 1133427 and 1702841 (EGL), NIH/COBRE P20GM109095 (JTO), NIH/INBRE P20GM103408 (JTO), NSF/CBET 1703466 (RAS), and NC State Game-Changing Research Incentive Program (RAS). The project described was supported by the National Center for Research Resources and the National Center for Advancing Translational Sciences, National Institutes of Health, through Grant TL1 TR001415 (RCN). The content is solely the responsibility of the authors and does not necessarily represent the official views of the NIH.

Funding information

Centers of Biomedical Research Excellence, Grant/Award Number: P20GM109095; Division of Chemical, Bioengineering, Environmental, and Transport Systems, Grant/Award Numbers: 1133427, 1702841, 1703466; IDeA Networks of Biomedical Research Excellence, Grant/Award Number: P20GM103408; National Center for Advancing Translational Sciences, Grant/Award Numbers: 550KR61325, 550KR71418, TR001415; National Institute of Biomedical Imaging and Bioengineering, Grant/Award Number: 1R03EB008790; National Stem Cell Foundation, Grant/Award Number: 15-059

DATA AVAILABILITY STATEMENT

The data that support the findings of this study are available from the corresponding author upon request.

REFERENCES

1. Cross M, Smith E, Hoy D, et al. The global burden of hip and knee osteoarthritis: estimates from the global burden of disease 2010 study. Ann Rheum Dis. 2014;73:1323–1330. [PubMed: 24553908]
2. Carbone A, Rodeo S. Review of current understanding of post-traumatic osteoarthritis resulting from sports injuries. J Orthop Res. 2017;35:397. [PubMed: 27306867]
3. Basad E, Wissing FR, Fehrenbach P, Rickert M, Steinmeyer J, Ishaque B. Matrix-induced autologous chondrocyte implantation (MACI) in the knee: clinical outcomes and challenges. Knee Surg, Sports Traumatol Arthrosc. 2015;23:3729–3735. [PubMed: 25218576]
4. Makris EA, Gomoll AH, Malizos KN, Hu JC, Athanasiou KA. Repair and tissue engineering techniques for articular cartilage. Nat Rev Rheumatol. 2015;11(1):21–34. [PubMed: 25247412]
5. Kwon H, Brown WE, Lee CA, et al. Surgical and tissue engineering strategies for articular cartilage and meniscus repair. Nat Rev Rheumatol. 2019;15:550–570. [PubMed: 31296933]
6. Khan IM, Gilbert SJ, Singhrao SK, Duance VC, Archer CW. Cartilage integration: evaluation of the reasons for failure of integration during cartilage repair. Eur Cells Mater. 2008;3(6):26–39.
7. Homicz MR, Schumacher BL, Sah RL, Watson D. Effects of serial expansion of septal chondrocytes on tissue-engineered neocartilage composition. Otolaryngol-Head Neck Surg. 2002;127:398–408. [PubMed: 12447233]
8. Nordberg RC, Loboa EG. Our fat future: translating adipose stem cell therapy. Stem Cells Transl Med. 2015;4:974–979. [PubMed: 26185256]
9. Sharma AR, Jagga S, Lee SS, Nam JS. Interplay between cartilage and subchondral bone contributing to pathogenesis of osteoarthritis. Int J Mol Sci. 2013;14:19805. [PubMed: 24084727]
10. Hung CT, Lima EG, Mauck RL, et al. Anatomically shaped osteochondral constructs for articular cartilage repair. J Biomech. 2003;36:1853–1864. [PubMed: 14614939]
11. Lima EG, Mauck RL, Han SH, et al. Functional tissue engineering of chondral and osteochondral constructs. Biorheology. 2004;41: 577–590. [PubMed: 15299288]
12. Schaefer D, Martin I, Shastri P, et al. In vitro generation of osteochondral composites. Biomaterials. 2000;21:2599–2606. [PubMed: 11071609]
13. Gotterbarm T, Richter W, Jung M, et al. An in vivo study of a growth-factor enhanced, cell free, two-layered collagen-tricalcium phosphate in deep osteochondral defects. Biomaterials. 2006;27: 3387–3395. [PubMed: 16488472]
14. Gotterbarm T, Breusch SJ, Jung M, et al. Complete subchondral bone defect regeneration with a tricalcium phosphate collagen implant and osteoinductive growth factors: a randomized controlled study in Göttingen minipigs. J Biomed Mater Res - Part B Appl Biomater. 2014; 102:933–942.
15. Mellor LF, Mohiti-Asli M, Williams J, et al. Extracellular calcium modulates Chondrogenic and osteogenic differentiation of human adipose-derived stem cells: a novel approach for osteochondral tissue engineering using a single stem cell source. Tissue Eng A. 2015;21: 2323–2333.
16. Tampieri A, Sandri M, Landi E, et al. Design of graded biomimetic osteochondral composite scaffolds. Biomaterials. 2008;29:3539–3546. [PubMed: 18538387]
17. Jiang J, Tang A, Ateshian GA, Guo XE, Hung CT, Lu HH. Bioactive stratified polymer ceramic-hydrogel scaffold for integrative osteochondral repair. Ann Biomed Eng. 2010;38:2183–2196. [PubMed: 20411332]
18. Kon E, Mutini A, Arcangeli E, et al. Novel nanostructured scaffold for osteochondral regeneration: pilot study in horses. J Tissue Eng Regen Med. 2010;4:300–308. [PubMed: 20049745]
19. Kon E, Delcogliano M, Filardo G, et al. A novel nano-composite multilayered biomaterial for treatment of osteochondral lesions: technique note and an early stability pilot clinical trial. Injury. 2010;41:693–701. [PubMed: 20035935]

20. Kon E, Delcogliano M, Filardo G, et al. Orderly osteochondral regeneration in a sheep model using a novel nano-composite multilayered biomaterial. J Orthop Res. 2010;28:116–124. [PubMed: 19623663]
21. Erisken C, Kalyon DM, Wang H. Viscoelastic and biomechanical properties of osteochondral tissue constructs generated from graded polycaprolactone and beta-tricalcium phosphate composites. J Biomech Eng. 2010;132:91013.
22. Lu HH, Subramony SD, Boushell MK, Zhang X. Tissue engineering strategies for the regeneration of orthopedic interfaces. Ann Biomed Eng. 2010;38:2142–2154. [PubMed: 20422291]
23. Mellor LF, Nordberg RC, Huebner P, et al. Investigation of multiphasic 3D-bioplotted scaffolds for site-specific chondrogenic and osteogenic differentiation of human adipose-derived stem cells for osteochondral tissue engineering applications. J Biomed Mater Res - Part B Appl Biomater. 2019;108:2017.
24. Mellor LF, Huebner P, Cai S, et al. Fabrication and evaluation of electrospun, 3D-bioplotted, and combination of electrospun/3D-bioplotted scaffolds for tissue engineering applications. Biomed Res Int Hindawi Limited. 2017;2017:1–9.
25. Nukavarapu SP, Dorcemus DL. Osteochondral tissue engineering: current strategies and challenges. Biotechnol Adv. 2013;31:706–721. [PubMed: 23174560]
26. Hurtig MB, Buschmann MD, Fortier LA, et al. Preclinical studies for cartilage repair: recommendations from the international cartilage repair society. Cartilage. 2011;2:137–152. [PubMed: 26069576]
27. Chu CR, Szczodry M, Bruno S. Animal models for cartilage regeneration and repair. Tissue Eng B, Rev. 2010;16:105–115.
28. Fisher MB, Belkin NS, Milby AH, et al. Cartilage repair and subchondral bone remodeling in response to focal lesions in a mini-pig model: implications for tissue engineering. Tissue Eng Part A. 2015;21: 850–860. [PubMed: 25318414]
29. McCullen SD, Stevens DR, Roberts WA, et al. Characterization of electrospun nanocomposite scaffolds and biocompatibility with adipose-derived human mesenchymal stem cells. Int J Nanomedicine. 2007;2:253–263. [PubMed: 17722553]
30. McCullen SD, Zhu Y, Bernacki SH, et al. Electrospun composite poly(L-lactic acid)/tricalcium phosphate scaffolds induce proliferation and osteogenic differentiation of human adipose-derived stem cells. Biomed Mater. 2009;4:035002. [PubMed: 19390143]
31. Haslauer CM, Moghe AK, Osborne JA, Gupta BS, Loboa EG. Collagen-PCL sheath-core bicomponent electrospun scaffolds increase osteogenic differentiation and calcium accretion of human adipose-derived stem cells. J Biomater Sci Ed. 2011;22:1695–1712.
32. Asli MM, Pourdeyhimi B, Loboa EG. Release profiles of tricalcium phosphate nanoparticles from poly(L-lactic acid) electrospun scaffolds with single component, core-sheath, or porous fiber morphologies: effects on hASC viability and osteogenic differentiation. Macromol Biosci. 2012;12:893–900. [PubMed: 22648935]
33. Bernacki SH, Wall ME, Loboa EG. Isolation of human mesenchymal stem cells from bone and adipose tissue. Methods Cell Biol. 2008;86: 257–278. [PubMed: 18442651]
34. Bodle JC, Teeter SD, Hluck BH, Hardin JW, Bernacki SH, Loboa EG. Age-related effects on the potency of human adipose-derived stem cells: creation and evaluation of Superlots and implications for muscu-loskeletal tissue engineering applications. Tissue Eng C, Methods. 2014;20:972–983.
35. Li WJ, Chiang H, Kuo TF, Lee HS, Jiang CC, Tuan RS. Evaluation of articular cartilage repair using biodegradable nanofibrous scaffolds in a swine model: a pilot study. J Tissue Eng Regen Med. 2009;3:1–10. [PubMed: 19004029]
36. Brittberg M, Aglietti P, Gambardella R, et al.ICRS Cartilage Injury Evaluation Package [Internett]. 2000.
37. Brittberg M, Winalski CS. Evaluation of cartilage injuries and repair. J Bone Jt Surg - Ser A. 2003;85:58–69.
38. Getgood A, Henson F, Skelton C, et al. Osteochondral tissue engineering using a biphasic collagen/GAG scaffold containing rhFGF18 or BMP-7 in an ovine model. J Exp Orthop. 2014;1(13):1–11. [PubMed: 26914746]

39. Levingstone TJ, Thompson E, Matsiko A, Schepens A, Gleeson JP, O'brien FJ. Multi-layered collagen-based scaffolds for osteochondral defect repair in rabbits. Acta Biomater. 2016;32:149–160. [PubMed: 26724503]
40. Im G Il, Ahn JH, Kim SY, Choi BS, Lee SW. A Hyaluronate-Atelocollagen/β-Tricalcium phosphate-hydroxyapatite biphasic scaffold for the repair of osteochondral defects: a porcine study. Tissue Eng - Part A. 2010;16:1189–1200. [PubMed: 19883204]
41. Pfeifer CG, Fisher MB, Saxena V, et al. Age-dependent subchondral bone remodeling and cartilage repair in a Minipig defect model. Tissue Eng Part C Methods. 2017;23:745–753. [PubMed: 28747146]
42. Christensen BB, Foldager CB, Olesen ML, et al. Experimental articular cartilage repair in the Göttingen minipig: the influence of multiple defects per knee. J Exp Orthop. 2015;2:1–11. [PubMed: 26914869]
43. Puetzer JL, Brown BN, Ballyns JJ, Bonassar LJ. The effect of IGF-I on anatomically shaped tissue-engineered menisci. Tissue Eng A. 2013; 19:1443–1450.
44. Mainil-Varlet P, Van Damme B, Nesic D, Knutsen G, Kandel R, Roberts S. A new histology scoring system for the assessment of the quality of human cartilage repair: ICRS II. Am J Sports Med. 2010;38:880–890. [PubMed: 20203290]
45. Matricali GA, Dereymaeker GPE, Luvten FP. Donor site morbidity after articular cartilage repair procedures: a review. Acta Orthop Belg. 2010;76:669. [PubMed: 21138224]
46. Awad HA, Wickham MQ, Leddy HA, Gimble JM, Guilak F. Chondrogenic differentiation of adipose-derived adult stem cells in aga-rose, alginate, and gelatin scaffolds. Biomaterials. 2004;25:3211–3222. [PubMed: 14980416]
47. Erickson GR, Gimble JM, Franklin DM, Rice HE, Awad H, Guilak F. Chondrogenic potential of adipose tissue-derived stromal cells in vitro and in vivo. Biochem Biophys Res Commun. 2002;290:763–769. [PubMed: 11785965]
48. Nordberg RC, Zhang J, Griffith EH, Frank MW, Starly B, Loboa EG. Electrical cell-substrate impedance spectroscopy can monitor age-grouped human adipose stem cell variability during osteogenic differentiation. Stem Cells Transl Med. 2017;6:502–511. [PubMed: 28191763]
49. McCullen SD, Zhan J, Onorato ML, Bernacki SH, Loboa EG. Effect of varied ionic calcium on human adipose-derived stem cell mineralization. Tissue Eng A. 2010;16:1971–1981.
50. Gao F, Chiu SM, Motan DAL, et al. Mesenchymal stem cells and immunomodulation: current status and future prospects. Cell Death Dis. 2016;7:e2062. [PubMed: 26794657]
51. Yañez R, Lamana ML, García-Castro J, et al. Adipose tissue-derived mesenchymal stem cells have in vivo immunosuppressive properties applicable for the control of the graft-versus-host disease. Stem Cells. 2006;24:2582–2591. [PubMed: 16873762]
52. Hoemann CD, Lafantaisie-Favreau CH, Lascau-Coman V, Chen G, Guzm an-Morales J. The cartilage-bone interface. [Internett]. J Knee Surg. J Knee Surg2012;25(2):85–98. [PubMed: 22928426]
53. Bonde HV, Talman MLM, Kofoed H. The area of the tidemark in osteoarthritis—a three-dimensional stereological study in 21 patients. APMIS. 2005;113:349–352. [PubMed: 16011661]
54. Vasara AI, Hyttinen MM, Pulliainen O, et al. Immature porcine knee cartilage lesions show good healing with or without autologous chondrocyte transplantation. Osteoarthr Cartil. 2006;14:1066–1074.

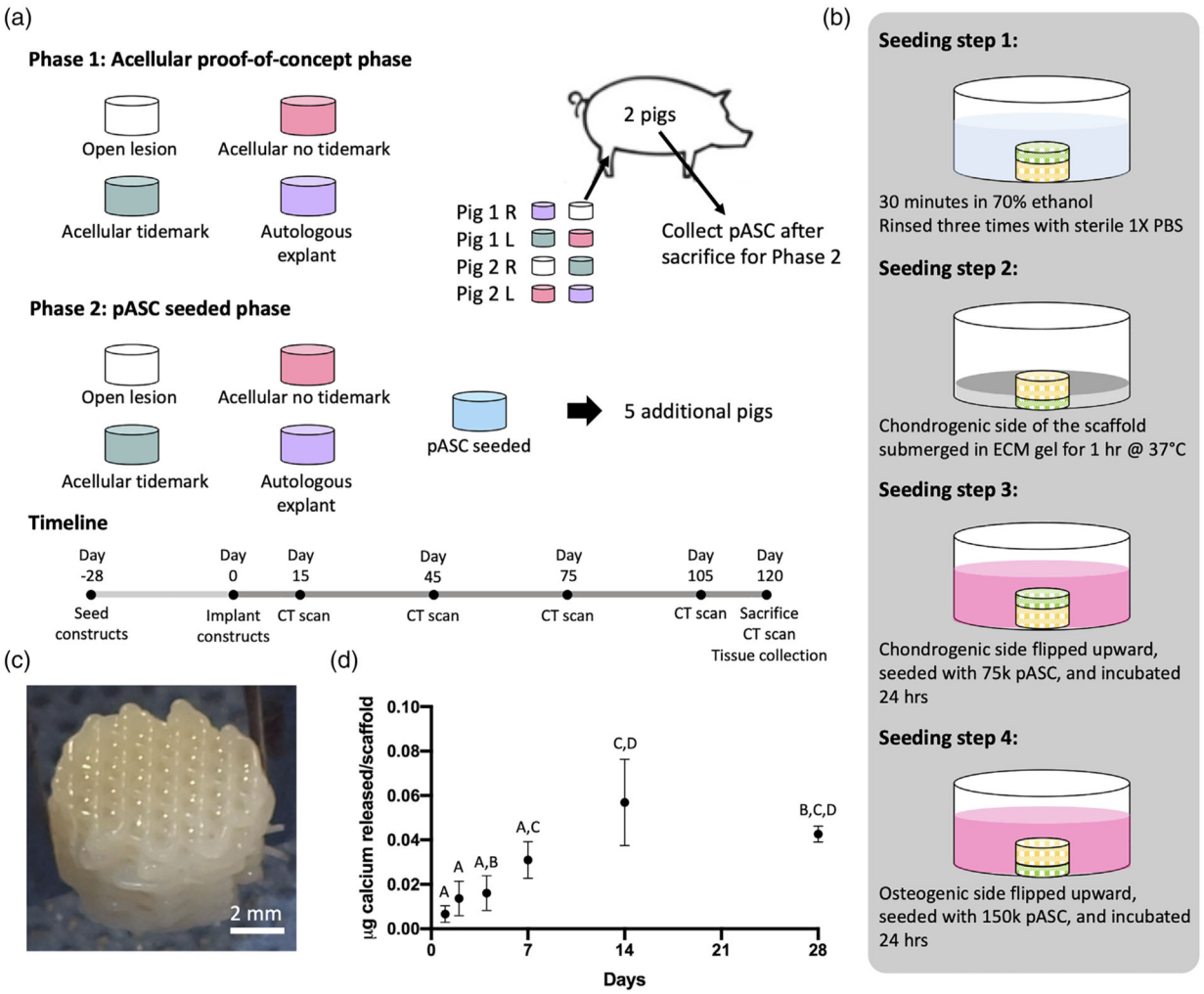

FIGURE 1.

(a) A schematic of the 2-phase experimental design and timeline. (b) Schematic of scaffold seeding method. (c) Osteochondral scaffolds consisting of a 100% PCL scaffold coated in a cartilage dECM gel (top), and a 80% PCL/20% TCP layer (bottom). (d) The calcium release characteristics of the scaffolds during 28-day in vitro culture. Bars represent mean + st. dev. Different letters indicate statistical difference ($p < 0.05$)

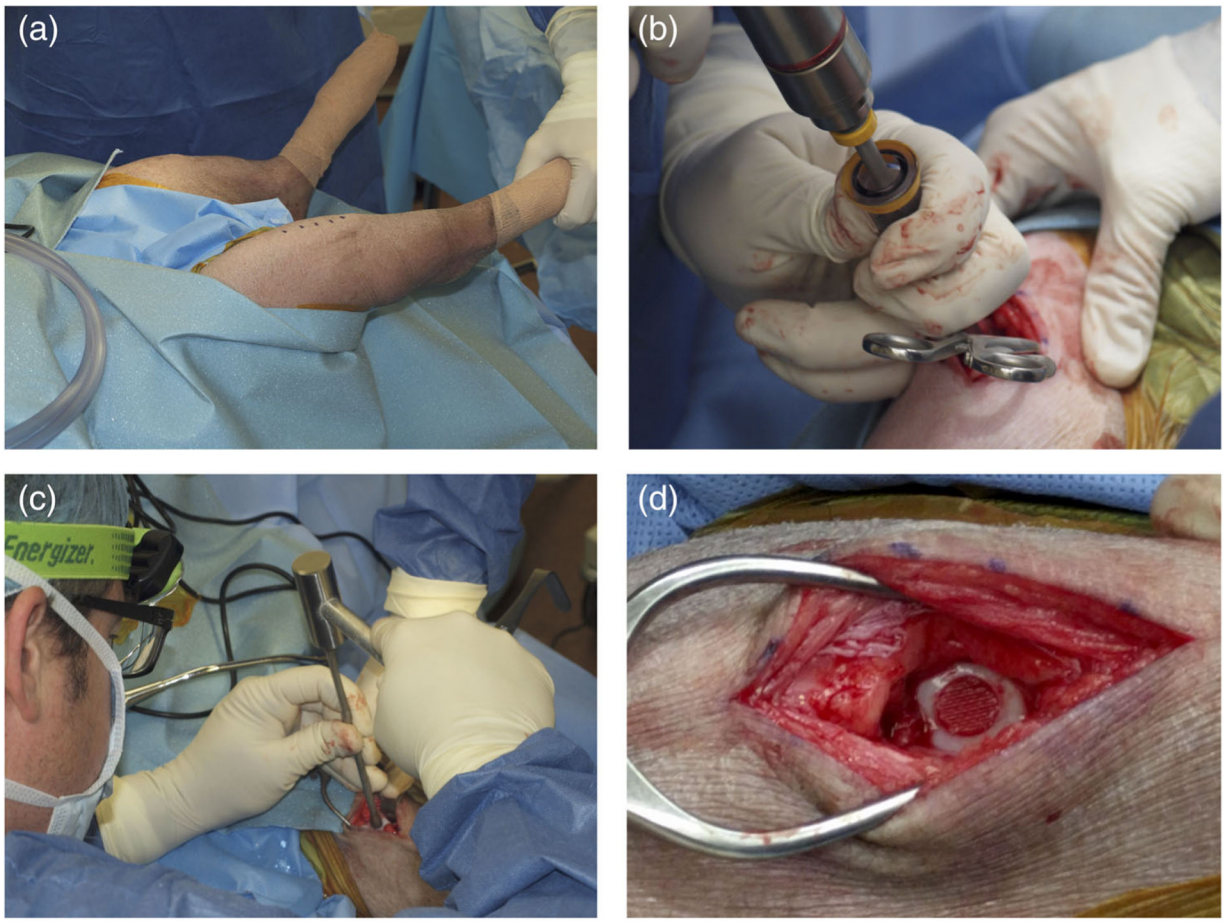

FIGURE 2.

Surgical method of scaffold implantation. (a) The minipigs were draped and surgical incision points were marked. (b) Osteochondral defects were generated. (c) The scaffolds were tapped into place with a mallet. (d) Once the scaffold was flush with the defect, the wound was sutured and bandaged

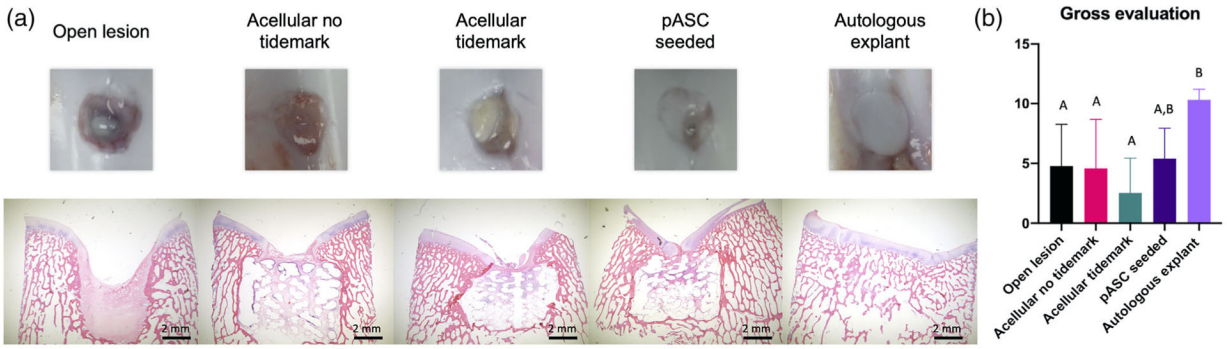

FIGURE 3.

Macro- and microscopic morphology of experimental groups 120 days after implantation. (a) Representative images of the gross morphology and corresponding H&E histological staining for each treatment group. (b) ICRS evaluation of the gross defect morphology. Bars represent mean + st. dev. Different letters indicate statistical difference ($p < 0.05$)

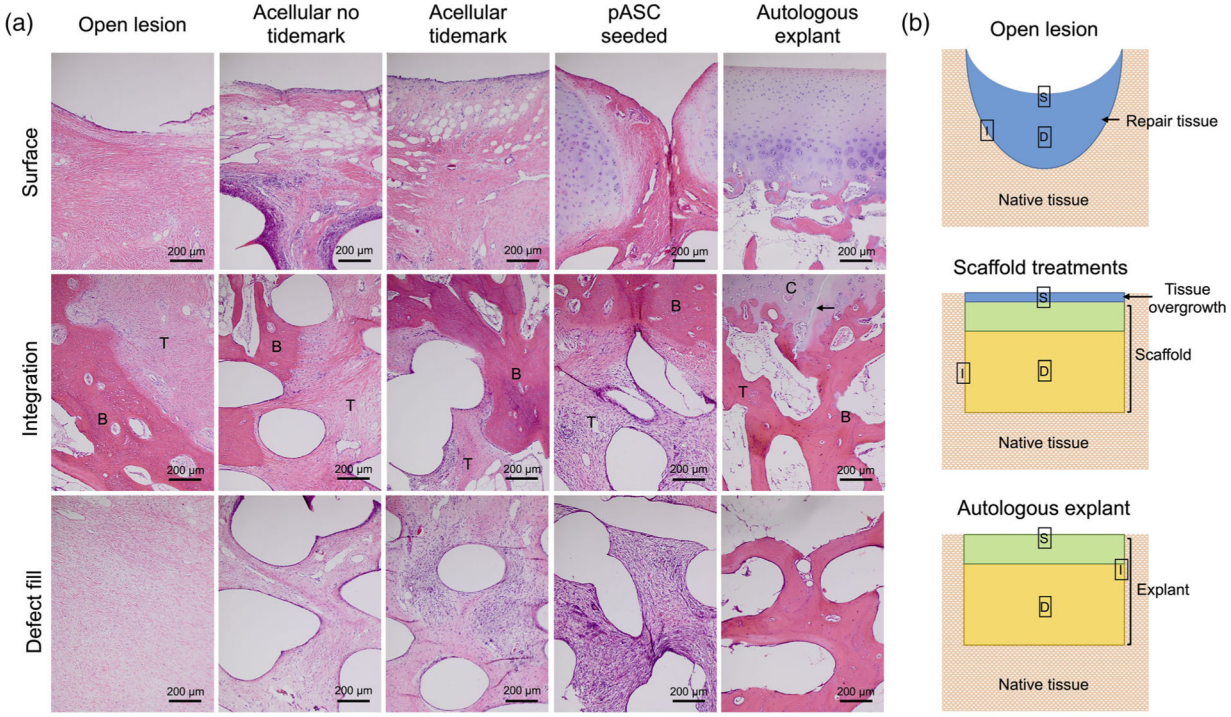

FIGURE 4.

(a) Magnified 10× H&E images of representative surface characteristics, treatment integration, and defect fill. B = native bone, T = treatment (scaffold, explant, or empty defect filled with repair tissue), C = cartilage, arrow indicates native/explant cartilage interface. (b) Diagram of locations from which the images were taken (S = surface, I = integration, D = defect fill)

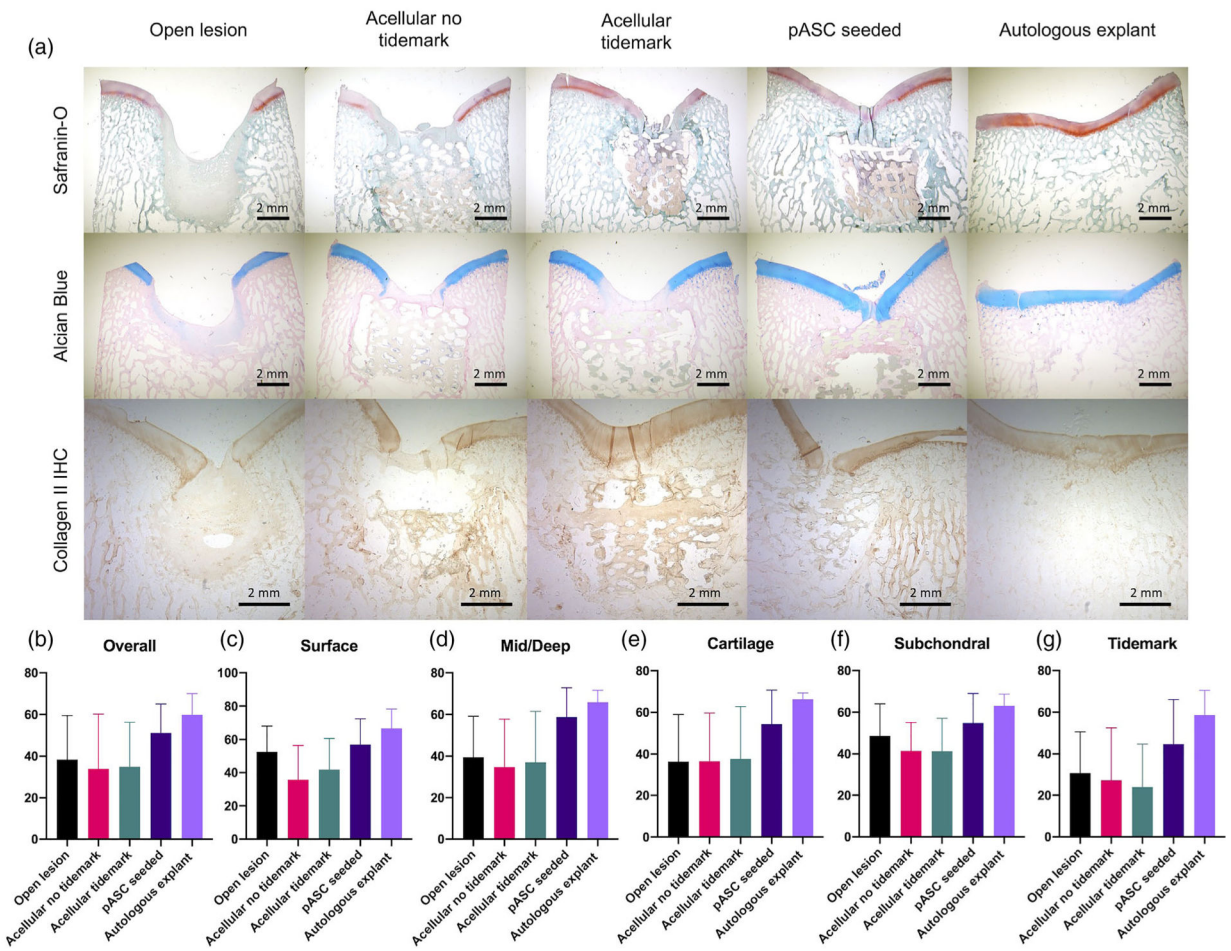

FIGURE 5.

Histological evaluation of controls and treatment groups. (a) Representative histological images of cartilage matrix staining via Alcian Blue and Safranin-O staining and collagen-II immunohistochemistry. (b-g) Scores given to each treatment via blind histological review using the ICRS II scoring system. Measures evaluated were (b) overall assessment, (c) surface/superficial assessment, (d) mid/deep zone assessment, (e) subchondral bone, (f) cartilage matrix staining, and (g) calcification front/tidemark. No statistically significant trends were observed (0 = worst, 100 = best). Bars represent mean + st. dev

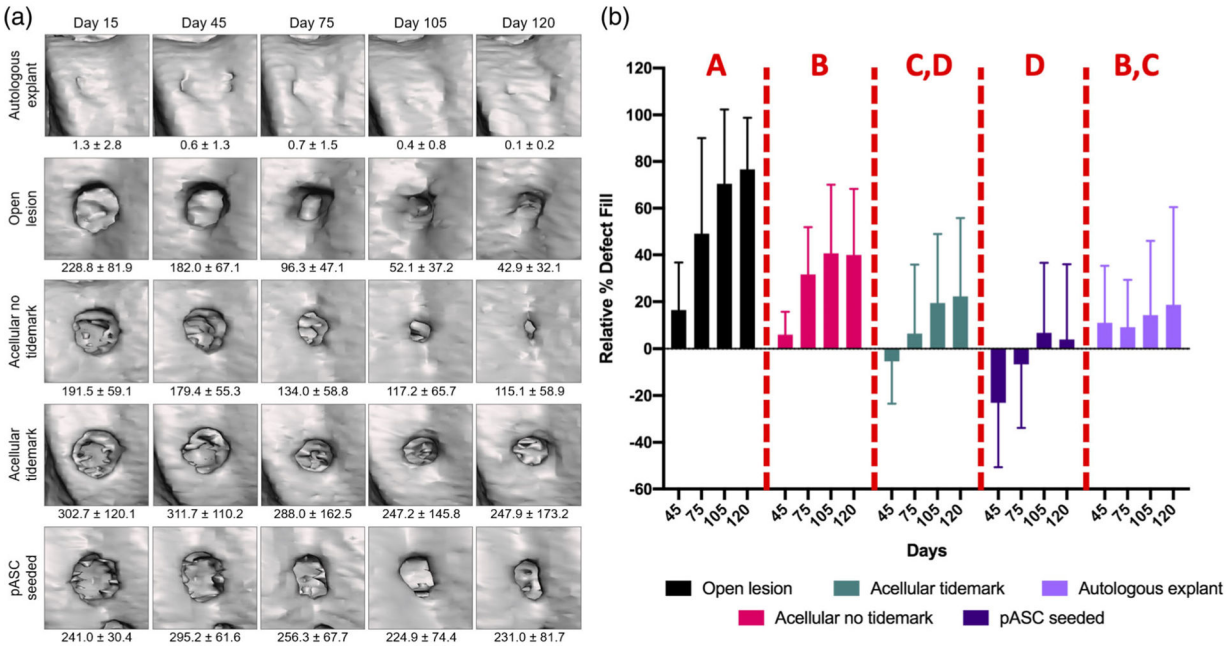

FIGURE 6.

CT evaluation of controls and treatment groups. (a) Representative samples of biomodels reconstructed from clinical CT data for each experimental group across all timepoints. For reference, the mean defect volume ± standard deviation (mm^3) are presented beneath each group. (b) Volumetric change of defects over time for all experimental groups. The relative defect fill is reported as the percent difference in volume from the original CTs collected at 15 days post-surgery. Bars represent mean + st. dev. Letter groups indicate statistical subsets for the experimental groups ($p < 0.05$)

TABLE 1

Design characteristics and 3D-bioplotting process parameters for each scaffold phase

			PCL 100 Chondrogenic phase	**PCL-TCP 80–20 Osteogenic phase**
DESIGN	Scaffold dimensions	Mm	Ø 7.9 × 2	Ø 7.9 × 4 w/chamfer
	Strand lay-down pattern	°	0-120-240	0-120-240
	Strand width	μm	350	350
	Interaxial strand separation	Mm	1	1
PROCESS	Extrusion temperature	°C	120	140
	Extrusion pressure	N/mm^2	0.6	0.6
	Printhead speed	Mm/s	1.2	0.9
	Extrusion nozzle diameter	Mm	0.3	0.3
	Layer height	Mm	0.32	0.32
	Preheat interval	min	20	20

J Biomed Mater Res B Appl Biomater. Author manuscript; available in PMC 2021 December 01.

TABLE 2

Relevant post-fabrication measures of scaffold characteristics at the microarchitectural and bulk levels

		Tidemark design	No tidemark design
Strand width	μm	356 ± 28	364 ± 32
Interstrand spacing	μm	607 ± 47	591 ± 44
Scaffold diameter	Mm	7.98 ± 0.11	7.98 ± 0.05
Scaffold height	Mm	7.17 ± 0.47	6.49 ± 0.04

TABLE 3

Summary of statistical significance between experimental groups and time points from the two-way ANOVA post-hoc analysis of percent defect fill, as plotted in Figure 6 (b). Bolding indicates statistical significance

Between experimental groups			**Between time points**		
Exp. group	**Exp. group**	**p-value**	**Time point**	**Time point**	**p-value**
Open lesion	Acellular no tidemark	**0.001**	Day 45	Day 75	**0.005**
	Acellular tidemark	**<0.000**		Day 105	**<0.000**
	pASC seeded	**<0.000**		Day 120	**<0.000**
	Autologous explant	**<0.000**	Day 75	Day 105	0.068
Acellular no tidemark	Acellular tidemark	**0.016**		Day 120	**0.020**
	pASC seeded	**<0.000**	Day 105	Day 120	0.970
	Autologous explant	0.072			
Acellular tidemark	pASC seeded	0.077			
	Autologous explant	0.993			
pASC seeded	Autologous explant	**0.035**			

J Biomed Mater Res B Appl Biomater. Author manuscript; available in PMC 2021 December 01.